Possible Mechanisms for Glacial Earthquakes

JOURNAL OF GEOPHYSICAL RESEARCH, VOL. 113, F03014, doi:10.1029/2007JF000944, 2008

Possible mechanisms for glacial earthquakes

Victor C. Tsai,[1] James R. Rice,[2] and Mark Fahnestock[3]

Received 7 November 2007; revised 9 June 2008; accepted 1 July 2008; published 5 August 2008.

[1] The large glacial earthquakes reported on by Ekström et al. (2003, 2006) and Tsai and Ekström (2007) have previously been evaluated in terms of their seismic characteristics. In this paper we attempt to take constraints such as known glacial ice properties, outlet glacier size, calving style, and meltwater variability to construct a self-consistent physical model of the glacial earthquake process. Since many glaciological parameters are poorly constrained, we parameterize a number of important processes and estimate a wide range of possible values for some properties. The range of model outputs is thus fairly large, but it is still difficult to match observational constraints under most conditions. We find that only a small class of models is able to satisfy the major observational constraints. These models are characterized by (1) lost basal resistance coupled to viscoelastic deformation with extensive internal crevassing or with low effective elastic modulus and possibly low effective viscosity or (2) by nonequilibrium calving, such as having large icebergs capsize into the glacier front. Although observational constraints cannot definitively rule out any of the proposed classes of mechanisms, the calving model has much stronger support. Fortunately, the various models make different predictions regarding observables that can potentially be measured in the near future.

Citation: Tsai, V. C., J. R. Rice, and M. Fahnestock (2008), Possible mechanisms for glacial earthquakes, *J. Geophys. Res.*, *113*, F03014, doi:10.1029/2007JF000944.

1. Introduction

[2] In 2003, *Ekström et al.* [2003] discovered a new class of earthquakes which they named glacial earthquakes because of their spatial association with glaciated regions. Since this initial discovery, *Ekström et al.* [2006] have reported on the strong seasonality and recent drastic increase in the number of Greenland glacial earthquakes, and *Tsai and Ekström* [2007] have performed a detailed seismic analysis of all 184 Greenland events detected between 1993 and 2005 (which composed roughly 95% of all known glacial earthquakes). Since events had radiation patterns inconsistent with standard double-couple faulting, seismic waveforms were modeled with the centroid single force (CSF) model of *Kawakatsu* [1989]. The CSF model accurately describes a mass sliding event (mass $\times$ distance) with an acceleration and then deceleration phase (beginning and ending at rest), and yielded satisfactory fits to the data [*Tsai and Ekström*, 2007]. (The model can alternatively be thought of as a pair of forces exerted on the Earth at the same location but offset in time and in opposite directions, e.g., as in the paper by *Dahlen* [1993].) This work resulted in a characterization of many seismic traits of Greenland events. Among the most important and robust conclusions of *Ekström et al.* [2003, 2006] and *Tsai and Ekström* [2007] are the following:

[3] 1. Glacial earthquakes primarily occur near the calving fronts of fast-flowing (>1 km a^{-1}) outlet glaciers.

[4] 2. They have mechanisms consistent with a near-surface horizontal temporally symmetric CSF approximately in the direction of local glacial flow.

[5] 3. All events detected have surface wave magnitude in the range $4.6 \leq M_{SW} \leq 5.1$ (M_{SW} is similar to the conventional M_S but is measured at 35–150 s [*Ekström*, 2006]). That corresponds to a CSF amplitude of 0.1×10^{14} kg m $\leq A \leq 2.0 \times 10^{14}$ kg m, with lower bounds corresponding with the detection limit.

[6] 4. They have significant energy in periods between 20 and 100 s (much longer durations than standard earthquakes of similar magnitude). The longer durations possibly correspond with larger amplitude events.

[7] 5. The presence of events is strongly seasonal and correlates with local conditions such as high surface temperature and the absence of thick sea ice mélange at the calving front.

[8] 6. Events occurring within the same outlet glacier do not all occur at the same location. The spread in locations is a factor of 2 larger than uncertainties and correlates with ice front variations.

[9] 7. Glacial earthquakes seem to have a characteristic amplitude dependent on which outlet glacier they are associated with.

[10] 8. To conclusions 1 to 7 we add the following: *Joughin et al.* [2008a] strongly suggest that glacial earthquakes are closely associated with calving events, with

[1]Department of Earth and Planetary Sciences, Harvard University, Cambridge, Massachusetts, USA.
[2]Department of Earth and Planetary Sciences and School of Engineering and Applied Sciences, Harvard University, Cambridge, Massachusetts, USA.
[3]Institute for the Study of Earth, Oceans, and Space, University of New Hampshire, Durham, New Hampshire, USA.

0148-0227/08/2007JF000944$09.00

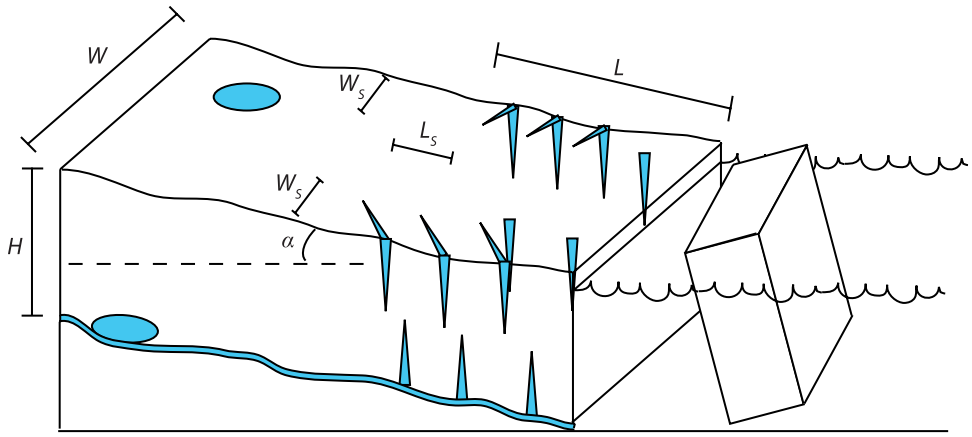

Figure 1. Schematic of processes modeled. We model ice deformation modulated by crevassing and fracture, basal processes modulated by hydraulic inputs, and calving of large icebergs. The mass affected has length L, width W, and height H, with ice deformation mostly confined to marginal shear zones and longitudinal deformation zone of size W_S and L_S, respectively.

glacial earthquakes occurring at times of large retreats of the calving front.

[11] Before the discovery of glacial earthquakes, a wide range of glacial seismic phenomena were known to exist [e.g., *Neave and Savage*, 1970; *VanWormer and Berg*, 1973; *Weaver and Malone*, 1979; *Wolf and Davies*, 1986; *Qamar*, 1988; *Anandakrishnan and Bentley*, 1993; *Anandakrishnan and Alley*, 1997; *Deichmann et al.*, 2000; *Stuart et al.*, 2005; *Smith*, 2006; *O'Neel et al.*, 2007], some of which have well-accepted mechanisms responsible for causing the seismicity (e.g., calving of icebergs, opening of crevasses, and basal slip are discussed in papers by *Qamar* [1988], *Deichmann et al.* [2000], *Stuart et al.* [2005], and *O'Neel et al.* [2007]). It is tempting to try to explain glacial earthquakes with a model known to describe one of these phenomena. But a number of difficulties arise in trying to quantitatively match glacial earthquake observations with the results of these models. For example, models that involve brittle crack propagation in ice [e.g., *Neave and Savage*, 1970] fail to correctly match the observed focal mechanism orientations, predict excitation at a shorter timescale than observed, and yield seismic energies much smaller than observed. Models involving basal slip of a segment of glacier [e.g., *Anandakrishnan and Alley*, 1997; *Bindschadler et al.*, 2003] fare better but still cannot achieve the large enough amplitudes or the 20–100 s timescales (with elastic models predicting much shorter timescales and viscous models predicting much longer timescales) without substantial modification of the model. Nevertheless some aspects of these models, such as the general block-sliding nature of the basal slip model, will be adopted and will factor heavily in our model. Current models involving calving [e.g., *O'Neel et al.*, 2007] similarly do not predict the correct timescales, mechanism orientations or energies, but further suggest that large calving events may be important to the generation of glacial earthquakes.

[12] The goal here is to construct a glaciologically consistent physical model of glacial earthquakes that satisfies the eight observational constraints listed above. We begin by incorporating, in general terms, the physics that we judge to be potentially relevant to the generation of glacial earthquakes. We formulate a general model framework in which ground motion (seismic signals) of various types can occur. We then utilize parameters constrained by observations such as 1, 5, and 8 and determine what range of values other, not as well constrained parameters of the model must have in order to satisfy or attempt to satisfy the other seismic observations 2, 3, 4, 6, and 7. Since constraints 6, 7, and parts of 5 do not have an obvious way in which to choose model parameters to satisfy them, we focus our efforts in this paper in satisfying conclusions 2, 3, and 4, and only afterward examine the ways in which the various classes of models are consistent with or would predict behavior described by conclusions 5, 6, and 7.

2. Model Inputs/Model Characterization

[13] There are a number of hypotheses regarding the specific physics governing glacial earthquakes [*Tsai and Rice*, 2006] including processes as diverse as shear failure of marginal ice, subglacial water pressures increasing to lift-off, transition of till to a rate-weakening regime, and stress changes induced by calving. Since, a priori, it is not possible to constrain which of these many possibilities can realistically produce the seismic observations, we take the conservative route of at first attempting to include, in general terms, all possibly relevant physics in our model of short-timescale terminus dynamics. Thus, we include ice deformation modulated by crevassing and fracturing, iceberg calving processes, and basal processes modulated by hydraulic inputs (schematically shown in Figure 1).

[14] The cost of including such a diverse set of physical processes is that in order to make progress we must, out of ignorance, neglect many of the details of the individual processes and focus instead on how the main effects of each contribute and interact to create a seismic signal consistent with those of glacial earthquakes. Moreover, a number of the processes listed are very poorly constrained and therefore must be parameterized instead of being modeled from first principles. A full description of the components of our model is in sections 2.1, 2.2, 2.3, 2.4, and 2.5. We allow for viscoelastic deformation of ice (section 2.1) that may be weakened by fracturing or other processes (section 2.2),

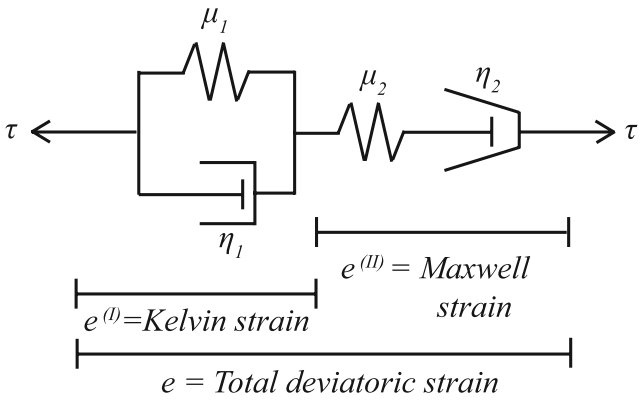

Figure 2. Schematic of the nonlinear Burger's body viscoelastic model used for deviatoric stress. The Maxwell viscosity η_2 is taken as nonlinear in accordance with Glen's law, and $e^{(I)}$ is the strain on the Kelvin element.

basal shear parameterized by a friction-like parameter that is a priori unconstrained (section 2.3), a variety of calving styles (section 2.4), and combine these into a self-consistent model framework applicable to the generation of a long-period seismic signal (section 2.5). A complete list of symbols used throughout this paper is provided in the Notation section.

2.1. Ice Deformation

[15] We recognize that deformation of ice within the outlet glacier is likely to be important to understanding glacial earthquakes. In glaciology it is common to treat ice deformation with a nonlinear viscous rheology described by Glen's law [*Glen*, 1955; *Paterson*, 2002]. However, for stress changes on the short timescale of interest to us, elastic deformation is also important [*Jellinek and Brill*, 1956; *Budd and Jacka*, 1989]. For clean, undamaged laboratory ice at timescales less than 100 s, only the instantaneous elastic modulus is important, at least at stresses that do not cause rapid fracture. However, since outlet glacier ice may have bulk viscoelastic-plastic and mechanical properties that differ substantially from those of laboratory specimens, we assume the more general Burger's body rheology that includes steady state and transient creep, as in papers by *Budd and Jacka* [1989] and *Kalifa et al.* [1992], i.e., a Kelvin element in series with a nonlinear Maxwell element as shown schematically in Figure 2. (The Kelvin response could, for example, represent effects of grain boundary sliding, the Maxwell response that of dislocation-dominated shear.)

[16] The stress-strain relations are such that the volumetric part of the total strain tensor response ε_{ij} is purely elastic (to the neglect of internal cavitation), whereas all time-dependent responses show up as contributions to the deviatoric part $e_{ij} = \varepsilon_{ij} - \delta_{ij}(\varepsilon_{xx} + \varepsilon_{yy} + \varepsilon_{zz})/3$ of the strain tensor. For the Burgers solid, we use $e_{ij} = e_{ij}^{(I)} + e_{ij}^{(II)}$ to represent the respective Kelvin (I) and Maxwell (II) contributions. Thus, neglecting material anisotropy,

$$\varepsilon_{ij} = \delta_{ij}\left(\sigma_{xx} + \sigma_{yy} + \sigma_{zz}\right)/(9K) + e_{ij}^{(I)} + e_{ij}^{(II)} \tag{1}$$

where $i, j = x, y, z$, σ_{ij} is the stress tensor, and bulk modulus $K = 2(1 + \nu)\mu_2/[3(1-2\nu)]$ where μ_2 is the shear modulus and ν the corresponding Poisson ratio for the instantaneous elastic response. Introducing the deviatoric stress tensor $\tau_{ij} = \sigma_{ij} - \delta_{ij}(\sigma_{xx} + \sigma_{yy} + \sigma_{zz})/3$, the deviatoric strain contributions satisfy

$$\tau_{ij} = 2\mu_1 e_{ij}^{(I)} + 2\eta_1 \dot{e}_{ij}^{(I)} \tag{2}$$

$$2\dot{e}_{ij}^{(II)} = \frac{\dot{\tau}_{ij}}{\mu_2} + \frac{\tau_{ij}}{\eta_2}. \tag{3}$$

[17] Here μ_1 is the shear modulus for the Kelvin response, such that the overall elastic shear modulus when the Kelvin response is fully relaxed is $(\mu_1^{-1} + \mu_2^{-1})^{-1}$ (the corresponding fully relaxed Poisson ratio differs from ν above; it is the value which keeps the bulk modulus K the same in the instantaneous and relaxed states). Also, η_1 and η_2 are the respective Kelvin linear viscosity and Maxwell nonlinear viscosity; we represent that nonlinearity as $\eta_2 = \eta_2(\tau)$ where $\tau = \sqrt{(1/2)\tau_{ij}\tau_{ij}}$ is the Huber-Mises equivalent shear stress, also known in the glaciological literature as the effective shear stress.

[18] Thus in uniaxial tensile or compressive stressing σ_{xx}, like for typical lab experiments, $\tau_{xx} = 2\sigma_{xx}/3$ and $\tau_{yy} = \tau_{zz} = -\sigma_{xx}/3$, so that $\tau = |\sigma_{xx}|/\sqrt{3}$ and the longitudinal and transverse strain rates are

$$\dot{\varepsilon}_{xx} = \dot{\sigma}_{xx}/[2(1+\nu)\mu_2] + \sigma_{xx}/\left[3\eta_2\left(|\sigma_{xx}|/\sqrt{3}\right)\right] + \dot{e}_{xx}^{(I)} \tag{4}$$

with

$$\sigma_{xx} = 3\mu_1 e_{xx}^{(I)} + 3\eta_1 \dot{e}_{xx}^{(I)} \tag{5}$$

and

$$\dot{\varepsilon}_{yy} = \dot{\varepsilon}_{zz} = -\nu\dot{\sigma}_{xx}/[2(1+\nu)\mu_2] - \sigma_{xx}/\left[6\eta_2\left(|\sigma_{xx}|/\sqrt{3}\right)\right] - \dot{e}_{xx}^{(I)}/2 \tag{6}$$

where $2(1 + \nu)\mu_2$ is recognized as the instantaneous Young's modulus. In pure shear stressing $\sigma_{xy} = \sigma_{yx}$, the shear strain rate is thus

$$\dot{\varepsilon}_{xy} = \dot{\sigma}_{xy}/(2\mu_2) + \sigma_{xy}/\left[2\eta_2\left(|\sigma_{xy}|\right)\right] + \dot{e}_{xy}^{(I)} \tag{7}$$

with

$$\sigma_{xy} = 2\mu_1 e_{xy}^{(I)} + 2\eta_1 \dot{e}_{xy}^{(I)}. \tag{8}$$

[19] We choose nominal values for the viscoelastic parameters to resemble laboratory measurements at temperate ice ($> -10°C$) conditions. We choose nominal values for μ_1, μ_2 and η_1 from experiments of *Jellinek and Brill* [1956] done in tension at $-5°C$ (the instantaneous elastic response has little temperature dependence [*Budd and Jacka*, 1989]). Modifying their values for use in shear instead of tensile deformation by assuming an instantaneous elastic Poisson's ratio $\nu = 0.3$ [*Vaughan*, 1995], we use $\mu_1 = \mu_2 = 2 \times 10^9$ Pa and $\eta_1 = 1 \times 10^{12}$ Pa s. In accordance with Glen's law, we take $\eta_2(\tau) = 2^{-1}A_{Gl}^{-1}\tau^{1-n}$ where $n \approx 3$ [*Glen*, 1955]. Glen's rate parameter A_{Gl} is highly temperature dependent, but for

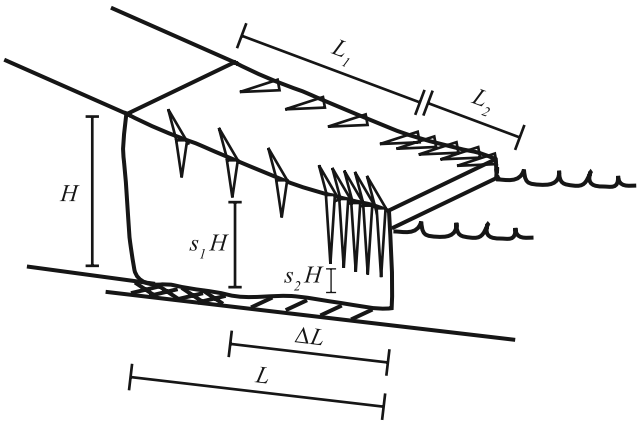

Figure 3. Schematic of crevassing and lost basal resistance. Extent of crevassing over length L_1 and L_2 is represented by s_1 and s_2, respectively. For this case, $s = (s_1L_1 + s_2L_2)/(L_1 + L_2)$. Basal resistance is lost over length ΔL.

nominal conditions and $n = 3$ we choose a constant, high value of $A_{GI} = 68 \times 10^{-25}$ s^{-1} (Pa)$^{-3}$ suggested as appropriate for temperate ice [*Paterson*, 2002] although this value is perhaps too high [*Truffer et al.*, 2001].

[20] The general form of the rheology (e.g., linear elasticity and power law viscous) dictates that the highest stresses, deformations and deformation rates are concentrated at the side margins and near the base (and at the edges of finite slipping patches of glacier) [e.g., *Nye*, 1965]. This fact is also confirmed by observations of large strain rate gradients across prominent outlet glaciers [*Joughin et al.*, 2004; *Howat et al.*, 2005]. In order to simplify the analysis greatly, we take the approximation of no deformation in the heart of the outlet glacier (block model) of width, height and length given by W, H and L, respectively, and with deformation concentrated into marginal shear zones, a basal shear zone and longitudinal deformation zones, of extent W_s, H_s and L_s, respectively (see Figure 1; note, later we shall choose $L_S = L/2$ to conservatively approximate a roughly constant longitudinal gradient in strain rate). Under a gravity-driven linear rheology, it is straightforward to calculate that over 50% of both viscous and elastic deformation is within 30% of the margins. Nonlinear effects such as Glen-like viscosity or deformation-induced fracture or shear heating enhance the degree to which the block model is a good approximation by further enhancing deformation near the edges. Using this approach, we necessarily average material properties over the appropriate length scale and only expect to predict observations quantitatively to within the degree to which the system is block-like.

2.2. Crevassing, Fracture, and Mechanical Weakening of Ice

[21] Fracturing and water content of ice both strongly affect the bulk viscoelastic properties and thus strongly modulate glacier flow. Some fracturing properties of ice are relatively well understood [e.g., *van der Veen*, 1998; *Rist et al.*, 1999; *Schulson*, 2001]. It is, for example, well known that surface crevasses in the outlet glaciers of interest can only extend to a depth of about 30 m unless the crevasses are filled with water, in which case crevasses can extend to the glacier base [e.g., *van der Veen*, 1998; *Das et al.*, 2008]. In contrast, the degree to which outlet glacier termini and margins are fractured englacially and water pervaded is only qualitatively known [e.g., *Kamb et al.*, 1994; *Venteris*, 1999; *Fountain et al.*, 2005; *Harper et al.*, 2005]. However, the terminus regions of these glaciers exhibit the highest tensile strain rates known to exist outside surges, and observations indicate that the ice is mechanically affected by internal damage.

[22] Fortunately, "steady state" velocity profiles, i.e., profiles estimated over timescales much longer than glacial earthquakes [e.g., *Howat et al.*, 2005], can give an estimate of the degree of weakening, whether this weakening is due to fracturing or other mechanisms (e.g., shear heating, fabric reorientation or increased water content). We find that performing a fit to transverse velocity profiles, $u(r)$, near the calving front with the approximation of *Nye* [1965] for a Glen's law rheology, $u(r) = u_0[1-(r/a)^{n+1}]$ for $-a < r < a$ where $2a$ = glacier width, yields a poor fit regardless of choice of u_0 (rms misfit of $\sigma = 1380$ m a^{-1}); but allowing for slip along the margins (constant velocity offset) in addition to the Glen's law rheology yields a better fit ($\sigma = 910$ m a^{-1}), with as much as 50% of the surface velocity being accommodated through slip at the margins. Farther from the front, however, a simple Glen's law rheology yields better fits ($\sigma = 460$ m a^{-1}), and adding marginal slip does not improve the fit. This simple calculation is in agreement with observations of near-marginal slip at other outlet glaciers [e.g., *Kamb et al.*, 1985].

[23] For the above reasons, we choose to spatially parameterize mechanical weakening by introducing a parameter $0 \leq s \leq 1$ that represents the fraction of the deforming regions over which the unweakened rheology is applied. Low s represents highly fractured, mechanically weakened ice. The average height over which shear stressing occurs, H_{eff}, can then be defined as $H_{eff} = sH$. Similarly, $H_{crev} = (1-s)H$ could be interpreted as the average height of crevasses or otherwise weakened ice (over which no shear stress is accommodated). Equivalently, s can be thought of simply as a scaling factor for viscoelastic parameters with e.g., $\mu_{2eff} = s\mu_2$ where μ_2 is the laboratory value and μ_{2eff} is the value appropriate for the region of the glacial system of interest, whether or not the physical reason for this scaling is due to crevassing. This scaling may, for example, be due to enhanced localized shear heating, high water content, or a softer fabric inherited from extensive straining [*Harrison et al.*, 1998]. As in other studies [e.g., *Vaughan*, 1995], there is a trade-off between s and μ_2 (and the other viscoelastic parameters). In our case this is because s enters the model multiplied by viscoelastic parameters (μ_1, μ_2, η_1, and η_2). Although it is likely that the margins are more crevassed relative to the rest of the glacier, and that the degree of crevassing also changes as one moves away from the calving front, in our simple rigid block model only the average value of s matters. So, for a length of glacier with s_1 over length L_1 and s_2 over length L_2, then $s = (s_1L_1 + s_2L_2)/(L_1 + L_2)$ (see Figure 3).

[24] Fracturing processes have two strong time dependencies that we address in our model of the relevant source mechanics for glacial earthquakes. The first effect is the seasonal variability of crevassing due to seasonal temperature variations. We expect more frequent and pervasive crevassing during summer months because of both the presence of liquid water, which aids in fracture propagation

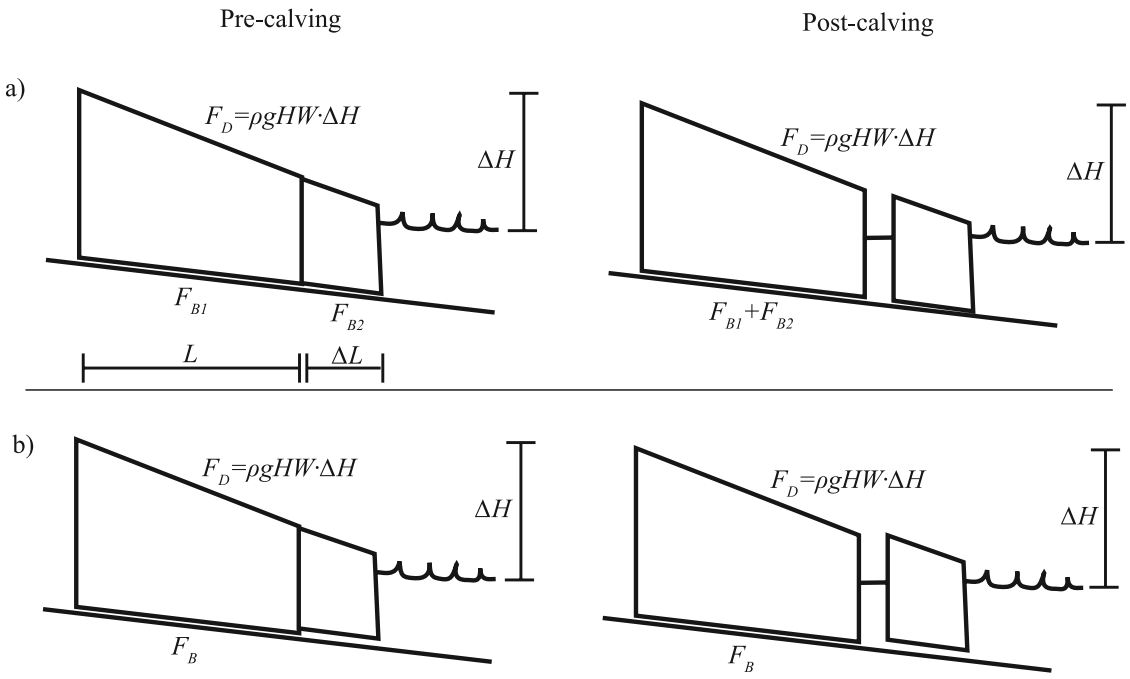

Figure 4. Schematic of the forces acting on the glacier precalving and postcalving, (a) with shear resistance on the precalved portion of glacier and (b) without shear resistance. The case shown in Figure 4a can be modeled with lost basal resistance; the case shown in Figure 4b has no net changes in forces.

[e.g., *van der Veen*, 1998; *Das et al.*, 2008], and decreased failure stress at higher temperatures [e.g., *Schulson*, 2001], which may be enhanced by existing crevasses and/or liquid water. The second effect is the increase in fractures caused by changes to the large-scale stress state in the terminus region potentially expected during a glacial earthquake event. Although both processes are easily understood qualitatively, and both imply more crevassing during times of glacial earthquakes, a quantitative physical description is not possible at this time. For this reason, we will discuss the possible implications of these processes as they fit into the broader model framework but leave a detailed physical model of these processes for future work. These processes also provide additional grounds for using viscoelastic parameters reduced from nominal values.

2.3. Basal Processes

[25] Modeling of surface velocity profiles [e.g., *Howat et al.*, 2005] with Glen's law suggests that, in the outlet glaciers of interest, a substantial fraction of their very high velocities are likely to be accommodated through both ice deformation and basal motion of some sort [e.g., *Truffer and Echelmeyer*, 2003] so an understanding of basal processes is required in a complete model of terminus dynamics. Unfortunately, it is currently not possible to resolve the detailed mechanics of basal motion. It is sometimes argued [e.g., *Truffer and Echelmeyer*, 2003] that it is unlikely for till to be responsible because till is presumed not to be able to withstand high shear stresses (often in excess of 100 kPa) inferred to exist at the base of these glaciers. However, that argument requires pore pressure conditions close to flotation whereas till with pore pressures less than lithostatic can sustain much higher shear stresses [e.g., *Tulaczyk et al.*, 2000]. It is unclear exactly how high pore pressures are in the locations we attempt to model. It is known that these glaciers are nearly thin enough to be at flotation at their termini but, at the base of a 1 km thick glacier, the pore pressure could be up to 98% of the ice pressure and potentially still sustain shear stresses of 100 kPa. It is also not clear exactly how high the shear stresses are very near the calving front. It has further been argued that most till would have been rapidly washed away by the active water system inferred to exist under these glaciers [*Iken et al.*, 1993], but this argument relies on properties of the basal water system which have not been well constrained. Thus, we shall assume both basal sliding and till deformation as well as any deformations associated with either to be plausible contributors to basal motion.

[26] Both basal sliding and till deformation have properties that can lead to a dramatic loss in shear strength over the tens of seconds during which glacial earthquakes occur [*Iken*, 1981; *Kamb*, 1991; *Schoof*, 2005]. (We will show that some model classes require such basal motion at the event timescale.) For example, the shear stress accommodated by both basal sliding and till deformation are proportional to some positive power of the effective pressure $p_{eff} = p_{ice} - p_w$ [*Paterson*, 2002] where p_{ice} = ice pressure and p_w = water pressure in a basal cavity system or within till, respectively. Thus, an increase of p_w to a large fraction of p_{ice} can cause dramatic weakening. This is essentially the argument of *Iken* [1981] for instability in sliding with a basal cavity system but the timescale must be set by hydraulic processes. The theory of *Kamb* [1991], on the other hand, yields an independent result for the timescale of instability (given by *Kamb* [1991, equation (32)]) though the model requires fairly extreme till properties as well as instantaneous adjustment of velocity perturbations to water pressure variations. In addition, further effects, such as rate-weaken-

ing till [e.g., *Kamb*, 1991], other transient rate-and-state effects [*Ruina*, 1983; *Tse and Rice*, 1986; *Dieterich*, 1994; *Lapusta et al.*, 2000; *Liu and Rice*, 2007], or fracture of basal ice resulting in lower basal roughness can result in unstable slip. As a result of these many possibilities, we simply assume that basal instability occurs over a length of glacier ΔL (see Figure 3) and determine a posteriori what form the basal instability must satisfy in order to satisfy observational constraints; we do not attempt to distinguish between basal sliding and bed deformation. In other words, we parameterize shear strength as $\tau = f(t) \cdot p_{ice}$ and allow the form of $f(t)$ to be fit by observations. It should be noted here that in section 3.1, $f(t)$ will be called upon to vary on timescales much faster than the fastest hydraulic changes currently documented in the literature [e.g., *Iken et al.*, 1983; *Kamb and Engelhardt*, 1987].

2.4. Calving

[27] We incorporate calving into our model as it can potentially produce a force resulting in a glacial earthquake. Direct observations [e.g., *Truffer et al.*, 2006; *MacAyeal et al.*, 2008] show that massive calving events exist and may produce large forces, and our model attempts to include a quantitative description of such events. If one defines calving as losing basal resistance to a portion of the glacier with no marginal shear forces then it can be modeled as above, with $L_2 = \Delta L$ and $s_2 = 0$, so we do not consider this option here. If, on the other hand, one defines calving as the fracture process that results in a crack separating the calved portion from the rest of the glacier, then calving can occur with the portion to be calved in one of three configurations: (1) (partially) grounded with basal traction, (2) partially grounded without basal traction but not neutrally buoyant, or (3) ungrounded and buoyant in water. If calving occurs under "equilibrium" conditions (i.e., without acceleration of either the calved portion or the remainder of the glacier) then the calved portion remains in the one of three configurations it started in. In case (1), the shear resistance previously taken up by the precalved portion must now be accommodated on the glacier side, thus transferring stress upstream (see Figure 4a). There is no net change in force on the glacier system as a whole but the transfer in stress is exactly equivalent to a complete loss of basal resistance over length ΔL being accommodated by increasing basal and marginal stressing over a length of glacier L (see Figure 4a). We therefore treat this case in the glacier motion framework outlined in sections 2.1, 2.2, and 2.3.

[28] In cases (2) and (3), there is no net change in force on the glacier since the precalving and postcalving water height is the same, yielding the same driving force, and the resistive shear forces are also identical (see Figure 4b). On the calved portion, the picture is different. For cases (1) and (2), there may be gravitational energy available allowing the calved portion to slide along its base, postcalving. However, only if the bed slope is sufficiently positive (in the same direction as the surface slope) can the calved portion accelerate away from the calving front (see Figure 5). The timescale for this process is given approximately by

$$T \approx \pi \sqrt{\frac{\rho H_C \cos\beta}{\rho_w g \sin^2\beta}} \tag{9}$$

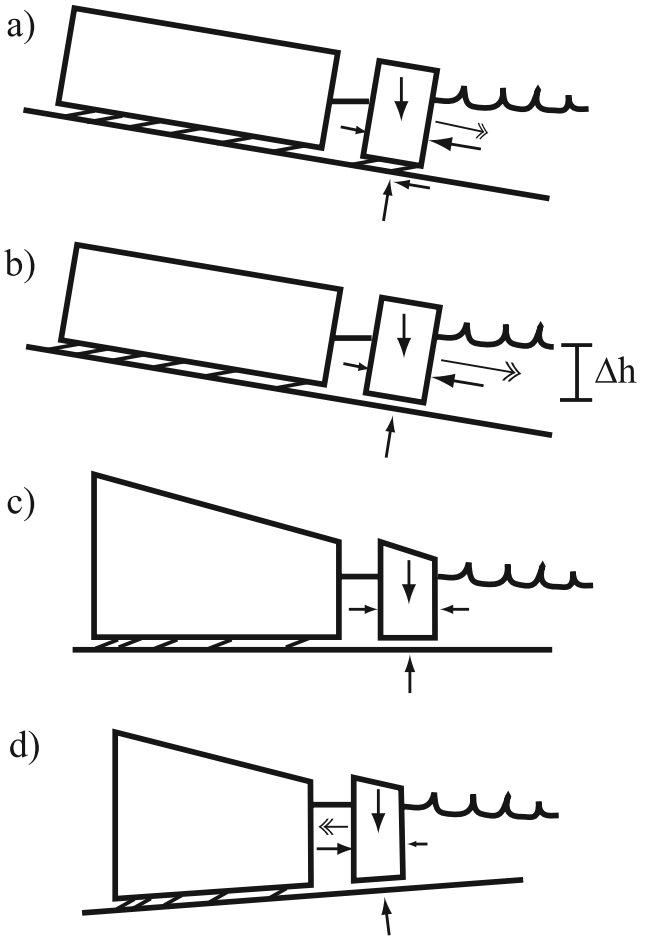

Figure 5. Schematic of the forces acting on the calved portion of glacier, (a) on a positive bed slope and with shear resistance, (b) on a positive bed slope without shear resistance, (c) on a horizontal bed, and (d) on a negative bed slope. Solid arrows denote forces, and double-headed arrows denote possible acceleration. Acceleration away from the calving front is only possible in cases shown in Figures 5a and 5b. In Figure 5b, Δh denotes the height of water to the middle of the base of the iceberg.

where we assume a rectangular cross section (Figure 5b) with side lengths H_C and L_C, with the latter in freely slipping contact with the bed, and where ρ = ice density, ρ_w = water density, g = gravitational acceleration, β = bed slope (see Appendix A). For $H_C > 500$ m and $\beta < 4°$, $T > 200$ s. Furthermore, observations [*Joughin et al.*, 2008a] imply that glacial earthquake events can occur on negative bed slopes. We therefore do not consider this possibility further. Finally, in case (3), there is no gravitational energy available so the iceberg has no net force on it.

[29] Since we have now considered all possibilities of equilibrium calving and rejected them as ways of producing a calving force, F_C, capable of generating a glacial earthquake, we require iceberg acceleration during the calving process to determine F_C. This acceleration must be approximately horizontal (with a dip angle of less than about 30 degrees) to match seismic observations [*Tsai and Ekström*, 2007]. A simple way in which this acceleration can occur is if the calved iceberg of dimensions H_C, W_C, L_C, is taller than

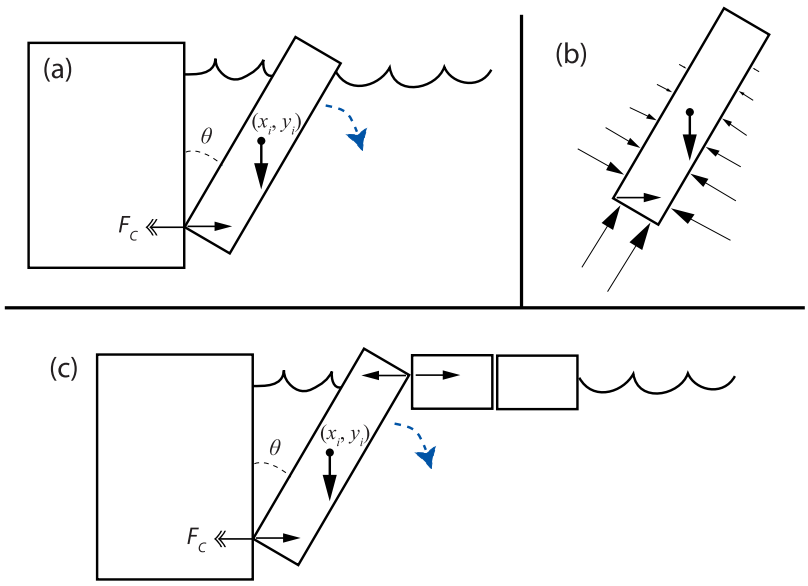

Figure 6. (a) Schematic of the tipping iceberg calving process modeled: the dotted arrow schematically denotes the rotation of the iceberg, the double arrow denotes the calving-contact force contributing to the seismic signal, and the solid arrows denote forces. (b) Force vectors acting on the calved iceberg. (c) Schematic of the tipping iceberg with a mechanically competent ice mélange.

it is long ($H_C > L_C$); it can tip over and possibly provide a force to the glacier front as in the model of *MacAyeal et al.* [2003]. Calving events of this type have been observed at a number of outlet glaciers [*Truffer et al.*, 2006; *O'Neel et al.*, 2007] but analysis of related seismicity has so far focused on short-period seismicity [*O'Neel et al.*, 2007] possibly associated with small slip events. To model the long-period character of this iceberg tipping process, we follow *MacAyeal et al.* [2003] except we allow for horizontal, vertical and rotational acceleration (see Appendix A for details). The system of equations we satisfy is

$$F_x = M_{xa}\ddot{x}_i \tag{10}$$

$$F_y = M_{ya}\ddot{y}_i \tag{11}$$

$$\tau_{rot} = I_a\ddot{\theta} \tag{12}$$

where x_i and y_i are mass center coordinates of the iceberg, forces are from gravity, hydrostatic water pressure and the calving-contact force at the glacier front (see Figure 6), τ_{rot} is torque, $\ddot{\theta}$ is angular acceleration, M_{xa} and M_{ya} are mass, and I_a is moment of inertia where M_{xa}, M_{ya} and I_a include "added mass" effects [*Lamb*, 1953; *Milne-Thomson*, 1955; *Brennen*, 1982]. In this first modeling effort, we approximate the flow as if it were remote from boundaries, and neglect surface wave dissipation and other edge effects due to the free surface and calving front. Preliminary modeling of these other effects shows that these effects cause significant but less than 1 order of magnitude changes to the amplitude and timescale. However, since the iceberg is near the free surface we ignore added mass effects in the vertical direction such that $M_{ya} = M_C = \rho W_C H_C L_C$. Horizontally, we use the rectangular block added mass formula of *Brennen* [1982] with height equal to the vertical cross-sectional height so that

$$M_{xa} \approx M_{xa0} \equiv \rho W_C H_C L_C + \frac{1.5\pi}{4}\rho_w W_C\left(H_C^2\cos^2\theta + L_C^2\sin^2\theta\right). \tag{13}$$

[30] Rotationally, we calculate the added moment of inertia from the elliptical formula of *Brennen* [1982], setting the major and minor axis lengths to the height and length of the rectangular block, respectively, so that

$$I_a \approx \frac{W_C}{24}\left[2\rho H_C L_C\left(H_C^2 + L_C^2\right) + \rho_w\left(H_C^2 - L_C^2\right)^2\right]. \tag{14}$$

[31] In the model, the calving-contact force is frictionless and thus exactly horizontal (so that iceberg weight is only supported by buoyant forces), $F_C = -F_x$, and only achieves positive (directed upstream) values; corresponding opposite momentum is delivered to the iceberg and ocean, and is transmitted to the solid Earth at much longer timescales by seawater viscosity. By default, the CSF model includes both an acceleration and deceleration phase of equal time, so the associated CSF timescale must be twice as long as the acceleration phase. Note that x_i, y_i and θ are not independent since contact is assumed (see Figure 6). The assumption of point-like contact is an obvious idealization but in this first modeling effort we assume a contact area that is small relative to iceberg size. The assumption of frictionless contact is also an obvious idealization; including the vertical shear forces associated with friction at the contact point may explain the small deviations from horizontal (up to 30 degrees) observed in reality [*Tsai and Ekström*, 2007]. Finally, one can derive a simple analytic expression for the CSF amplitude A (mass times distance moved) and timescale T of this process by approximating the system as an inverted pendulum driven by

its own buoyant weight over the horizontal distance traveled. The CSF amplitude is given by

$$A \approx 0.5\, M_C(H_C - L_C) = 0.5\rho W_C L_C H_C (H_C - L_C). \quad (15)$$

[32] Writing the pendulum equation as $(T/2\pi)^2\ddot{\theta} - \sin\theta = 0$ ($\theta = 0$ being an unstable equilibrium) then the characteristic timescale is given by

$$T \approx 2\pi\sqrt{\frac{\rho H_C}{(\rho_w - \rho)g}} \quad (16)$$

(although the actual time is dependent on initial conditions).

[33] The calving model discussed above is just one possible way in which iceberg acceleration can occur. There are potentially many other scenarios including, for example, one in which the iceberg impacts the fjord bed (J. Amundson, private communication, 2008); but we shall discuss just one variation on the above theme that involves the mélange of icebergs that often floats in front of the glacier. Although this iceberg mélange is typically composed of many individual bergs, it has been observed to act somewhat mechanically competent [e.g., *Truffer et al.*, 2006], with forces capable of being transmitted across km of icebergs with little time delay. If a calving event, such as the tipping event previously described, pushes into this mélange, it can potentially resist motion much more than the added mass effects of just the water. We therefore allow for this mélange added mass (which affects only the horizontal acceleration if the mélange is confined to move horizontally) by including a second contact force $F_{C2} = M_M(2\ddot{x}_i)$. Here, $2x_i$ is the distance between contact points and M_M is the effective mass from the iceberg mélange (see Figure 6c), which is used as a parameter in subsequent simulations. This is equivalent to modifying M_{xa} in equation (10) to be

$$M_{xa} \approx M_{xa0} + 2M_M \quad (17)$$

where M_{xa0} is the original effective mass in the x direction as in equation (13). In contrast to the simple tipping calving model which yields identical forces whether the iceberg tips bottom out or top out, the model with an iceberg mélange only has a simple interpretation when the iceberg tips top out (see Figure 6c). The interpretation is not obvious when the iceberg tips bottom out but net mélange motion must eventually be comparable since similar volume must still be vacated for the tipped iceberg.

2.5. A Unifying Model of Outlet Glacier Termini Forces

[34] We have thus far described how ice deformation, fracture of ice, basal processes and calving dynamics can affect the generation of glacial earthquakes. We now incorporate these effects into a single model that results in a prediction of the seismic force history. In addition to the calving-contact force at the glacier tongue, the resistive forces arising from ice deformation and basal "friction," we also have a driving force from gravity given by $F_D \approx \rho g\alpha \cdot HWL$ (which we take as constant through a seismic event since the total height differential $\alpha \cdot L$ responsible for the driving force is minimally affected by the event). Combining these processes, we obtain an expression for the glacier block acceleration $\ddot{x}_b$:

$$M\ddot{x}_b = F_D - F_M - F_B - F_L - F_C \quad (18)$$

where M = mass of glacier block, F_M = marginal shear force, F_B = basal shear force, F_L = longitudinal force (positive if tensile) at upstream end of block, and F_C = calving-contact force. The change in force on the (nonglacial) solid Earth, which generates a seismic response, is given by:

$$F_S(t) = F_M(t) + F_B(t) + F_L(t) - F_M(0) - F_B(0) - F_L(0) \quad (19)$$

[35] Since we treat F_D as constant, and initially $\ddot{x}_b = 0$ and $F_C(0) = 0$, then equivalently:

$$-F_S(t) = M\ddot{x}_b + F_C(t) \quad (20)$$

[36] In general, then, the seismic force can be thought of as having contributions from acceleration of the glacier and from acceleration of the calved iceberg. Since F_C is expected to always be nonnegative (directed upstream), the two contributions reinforce only when $\ddot{x}_b$ is positive (downstream acceleration). However, positive F_C only contributes to F_S when $\ddot{x}_b = 0$ and simply decreases $\ddot{x}_b$ when $\ddot{x}_b > 0$. Thus, in the following analysis we consider the two cases separately in 2 distinct model classes. That is, in class I models glacial earthquakes result from perturbations in glacier motion, and we set $F_C = 0$. In class II models glacial earthquakes result from iceberg calving, and we set $\ddot{x}_b = 0$.

[37] In class I models, the forces F_M and F_L can be calculated in terms of the motion history $x_b(t)$ using the viscoelastic framework and simplified deformation of section 2.1. That is, we use the rheology described in equations (7) and (8) for $F_M(t)$ with $\varepsilon_{xy} = x_b/(2W_S)$ and equations (7) and (8) with all stresses multiplied by 3 to approximately account for tensile rather than shear stressing for $F_L(t)$ with $\varepsilon_{xx} = x_b/L_S$. (For downslope horizontal stress change with no vertical change and plane strain constraint in the transverse horizontal direction, the elastic stiffness is $2\mu_2/(1-\nu) \approx 3\mu_2$.) We additionally prescribe $F_B(t)$ (representing a drop in strength) and set $F_C = 0$. With expressions for these forces substituted, we solve equation (18) for $x_b(t)$ with initial conditions $x_b(0) = x_{b0}$, $\dot{x}_b(0) = u_{ss}$ = steady state speed, and substitute into equation (20) to solve for $F_S(t)$.

[38] In class II models, we solve equations (10), (11), and (12) for x_i and y_i with initial conditions $x_i(0) = x_{i0}$, $y_i(0) = y_{i0}$, $\dot{x}_i(0) = 0$, $\dot{y}_i(0) = 0$ corresponding to a rotationally unstable iceberg. Equation (10) then gives $F_x = -F_C$ which can be substituted into equation (20) to solve for $F_S(t)$. Once $F_S(t)$ is known, the CSF amplitude is easily obtained by double integration in time:

$$A = \int_0^T \dot{A}(t)dt = \int_0^T \int_0^t F_S(t')dt'dt \quad (21)$$

2.6. Physical Constraints

[39] The size of outlet glaciers and the background surface velocity profiles are relatively well constrained by observations [e.g., *Joughin et al.*, 2004; *Howat et al.*, 2005]. Model parameter values are unique for individual glaciers, but typical values are on the order of $\alpha \leq 4°$ (usually $\alpha \leq 2°$), $W_S \leq 2$ km, $u_{ss} \approx 8$ km a^{-1}, $H \approx 1$ km, $W \approx 4$ km, $\Delta L \leq$

$L \leq 30$ km, and $A_{Gl} = 68 \times 10^{-25}$ s^{-1} (Pa)$^{-3}$ [*Bamber et al.*, 2001; *Paterson*, 2002; *Joughin et al.*, 2004; *Howat et al.*, 2005]. We shall use these representative values with $\alpha \approx 0.02 \approx 1°$, $W_S \approx 1$ km and $\Delta L = L$ for the rest of this paper. (Note that choosing $\Delta L < L$ would result in a lower-amplitude response.) In steady state, these parameter choices result in $F_L \approx 0$, $F_D \approx 180$ kPa $\times LW$, $F_M \approx 270$ kPa $\times LH_{eff}$ and 40 kPa $\times LW \leq F_B \leq 180$ kPa $\times LW$. This estimate for F_B leads to an estimate of the initial dimensionless basal shear strength $f(0) = f_0$ as $0.005 \leq f_0 \leq 0.02$. However, the estimates for F_B and f_0 are both quite sensitive to the choice of W_S, which is not well constrained.

3. Model Results

[40] If we attempt to model a glacial earthquake without the inclusion of calving, relying on only block-like glacier motion (like in Figure 3), and assume nominal material property values, then the correct amplitude and timescale cannot be achieved. That is, choosing $\mu_1 = \mu_2 = 2 \times 10^9$ Pa, $\eta_1 = 1 \times 10^{12}$ Pa s, $n = 3$, $A_{Gl} = 68 \times 10^{-25}$ s^{-1} (Pa)$^{-3}$, $L = \Delta L = 5$ km, $L_S = L/2$, $s = H_{eff}/H = 1$, $F_C(t) = 0$ and with an instantaneous drop of $f(t)$ from f_0 to zero then, at timescales less than 10^3 s, only the elastic term (μ_2) is important and we achieve CSF amplitudes of $A = 1.1 \times 10^{12}$ kg m over a timescale of $T = 2.5$ s. An analytic approximation for this elastic response can also be obtained from a simple elastic force balance (see Appendix A) which yields:

$$A \approx \frac{\rho^2 g H W^2 W_S \cdot \Delta L}{s\mu_2[1 + 3WW_S/(2LL_S)]} \cdot \left[\alpha - \frac{2s}{\rho g W}\left(\frac{u_{ss}}{2W_S A_{Gl}}\right)^{1/3}\right] \quad (22)$$

and

$$T \approx \pi\sqrt{\frac{2\rho WW_S LL_S}{s\mu_2(3WW_S + 2LL_S)}}. \quad (23)$$

[41] The amplitude is 10 to 200 times smaller than observations and the timescale is eight to 40 times too short. If we have successfully included all the physics pertinent to the generation of glacial earthquakes, then the only way in which observations can be matched is to modify at least one of the model parameters from its nominal value. We take ρ, g, and W to be well constrained by observations, leaving α, H, L, ΔL, μ_1, μ_2, η_1, A_{Gl}, W_S, H_S, L_S, s, $f(t)$, and $F_C(t)$ as at least partially adjustable parameters.

3.1. Class I Models: Seismogenesis by Glacier Block Acceleration

[42] In this class of models, we keep $F_C(t) = 0$ (seismogenesis in the absence of calving) for reasons discussed in section 2.5. We also choose to include longitudinal deformation only on the upstream side of the sliding glacier block (and terminating in open waters on the other) since it requires less change from nominal values and is strongly suggested by observation 8. In order to achieve CSF amplitudes of 0.4×10^{14} kg m (median value for glacial earthquakes) we require a combination of decreasing μ_1, μ_2, η_1, and s or increasing ΔL, L_S, W_S, A_{Gl} and α. Setting $\mu_2 = 5 \times 10^7$ Pa (versus lab value of 2×10^9 Pa) or $s = 0.2$ can individually account for the observed CSF amplitudes whereas changes in μ_1, η_1, ΔL, L_S, W_S, A_{gl} or α alone cannot. Large decreases in μ_1 and η_1 (e.g., $\mu_1 = 2.5 \times 10^7$ Pa and $\eta_1 = 5 \times 10^8$ Pa s versus lab values of 2×10^9 Pa and 1×10^{12} Pa s, respectively) must be coupled in order to have a significant effect; increases in L_S and W_S also must be coupled but W_S is constrained to less than 2 km; increases in A_{Gl} only increase the proportion of resistance taken up by the bed initially in steady state and is also constrained to less than 200×10^{-25} s^{-1} (Pa)$^{-3}$; ΔL and α are constrained in section 2.6. In order to achieve timescales of 50 s, we require choosing timescales of variation in $f(t)$ close to 50 s; choosing very low values of μ_2 with possibly low values of s ($\mu_2 = 5 \times 10^6$ Pa or $\mu_2 = 2 \times 10^7$ Pa and $s = 0.2$); or choosing 10 s $\leq \eta_1/\mu_1 \leq 20$ s. While some of these choices are perhaps on the extreme side of plausible, all of the suggested changes in parameter values are made to variables with sufficiently uncertain field values to warrant at least an examination of the possibility of a value different from nominal of the extent chosen.

[43] In principle, there are infinite combinations of choices that will result in an amplitude and timescale consistent with seismic observation. For example, one could choose (as values different than nominal) $\Delta L = 9$ km, $\mu_2 = 5 \times 10^8$ Pa, $W_S = 1.5$ km, $s = 0.5$ and $f(t)$ varying on a 50 s timescale to satisfy observations. However, certain parameter sets require fewer changes from nominal values, or contain pairs of changes that are physically paired (coupled). Thus, we focus our attention on three subclasses of models that satisfy the amplitude and timescale constraints. All three subclasses require changes in $f(t)$. In two of the three subclasses, we assume the form of $f(t)$ can be chosen arbitrarily to fit timescales set by a variety of glaciological processes (such as subglacial hydraulic flow) whose short-time behavior are rather unconstrained. This philosophy is different than the one typically taken in earthquake modeling where the frictional time dependence is an outcome of the analysis, on the basis of a specified constitutive law. Before turning to these three subclasses, we note that although the dependence of amplitude and timescale on the parameters is nonlinear, we can linearize the model and find the first-order response away from the nominal values. This linear response provides guidance for our parameter choices, and is given in Table 1.

3.1.1. Model IA: Highly Fractured, Timescale Set by Basal Strength *f(t)*

[44] In this subclass of models, we choose nominal viscoelastic parameters. In order to achieve correct amplitudes we can, for example, set $\Delta L = L = 5.5$ km and $s = 0.2$. In order to achieve correct timescales (20–100 s), we must utilize the timescale controlling basal motion $f(t)$ so that for example

$$f(t) = \begin{cases} f_0 & t < 0, t > 2t_0 \\ f_0/2 \cdot [1 + \cos(\pi t/t_0)] & 0 < t < 2t_0 \end{cases} \quad (24)$$

where $t_0 \approx 50$ s. In this case, the time dependence of the glacial earthquake is completely governed by a process (loss of basal resistance) that (in our model) has a completely unconstrained time history, and we therefore set it to match timescale observations.

3.1.2. Model IB: Very Low Maxwell Shear Modulus μ_2, *f(t)* Regains Strength

[45] Choosing $\Delta L = 2.2$ km, $W_S = 500$ m and $\mu_2 = 1.6 \times 10^6$ Pa (and nominal other values) generates correct ampli-

Table 1. Linear Response of Amplitude and Timescale to Block Acceleration Parameters

Parameter	Amplitude Response	Timescale Response
α	38×10^{11} kg m/°	0
H	11×10^{11} kg m/km	0
ΔL	2.9×10^{11} kg m/km	0.1 s/km
μ_1	0	0
μ_2	-29×10^{11} kg m/$\Delta\log_{10}$Pa	-3.1 s/$\Delta\log_{10}$Pa
η_1	-0.12×10^{11} kg m/$\Delta\log_{10}$(Pa s)	0
A_{Gl}	24×10^{11} kg m/$\Delta\log(s^{-1}\ Pa^{-3})$	0
W_S	18×10^{11} kg m/km	3.4 s/km
H_S	0	0
L_S	1.1×10^{11} kg m/km	0.1 s/km
s	-46×10^{11} kg m/1	-1.6 s/1
$f(t)$	0	1s/1s

tudes and timescales but the spring is under-damped so in order to have only one oscillation, $f(t)$ must jump back to f_0 after 50 s, e.g.,

$$f(t) = \begin{cases} f_0 & t < 0\text{s}, t > 50\text{s} \\ 0 & 0\text{s} < t < 50\text{s} \end{cases}. \quad (25)$$

[46] Many seismic waveforms are in fact consistent with a multiple oscillation signal, so there is a certain leeway in exactly how long $f(t)$ drops to zero. In this case, the ice would be allowed to slide back uphill, which seems peculiar but could not be precluded if there were sliding on a fully fluid layer. For example, using

$$f(t) = \begin{cases} f_0 & t < 0 \\ f_0 \cdot [1 - \exp(-t/150\text{s})] & t > 0 \end{cases} \quad (26)$$

would also satisfy observations. As in Model IA, the timescale is partially set by the timescale of a process that has an unconstrained timescale in our model. It is perhaps worth noting, though, that with rate- and state-dependent friction as in earthquake studies [e.g., *Ruina*, 1983], this general strengthening behavior may be expected when sliding velocity diminishes significantly.

3.1.3. Model IC: Low Kelvin Shear Modulus μ_1 and Low Associated Viscosity η_1

[47] The final end-member of parameter choices is to modify both η_1 and μ_1 to values substantially lower than nominal, i.e., $\mu_1 = 2.5 \times 10^7$ Pa and $\eta_1 = 5 \times 10^8$ Pa s and drop $f(t)$ to zero. Here, η_1/μ_1 is chosen to match the timescale desired and we no longer require $f(t)$ to accommodate this timing. Note that these drastic changes from nominal values are perhaps warranted if the ice is effectively weakened by fracture or other mechanisms.

3.2. Class II Model: Seismogenesis by Calving of Large Icebergs

3.2.1. Model IIA: Calving of Rotationally Unstable Icebergs

[48] As an alternative to the class I set of models, where glacier acceleration is responsible for the seismic force, here the calving-contact force is directly responsible and assumed to couple directly to the solid Earth without acceleration of the glacier ($\ddot{x}_b = 0$). We use the calving model described in section 2.4. Without modification, neutrally buoyant initial conditions and with iceberg dimensions H_C = 500 m, W_C = 5 km, L_C = 265 m, this model (IIA) produces approximately the correct amplitude and a slightly long timescale. These choices for H_C, W_C, L_C and were taken to best fit the amplitude and timescale constraints; for example, the rather exact value of L_C chosen is due to the sensitivity of both amplitude and timescale to both H_C and L_C as in accord with equations (15) and (16). The model of iceberg tipping also matches observations of calving style [*Truffer et al.*, 2006; J. Amundson, private communication, 2008] of some large calving events, which have been observed to tip both bottom out and top out. In Figure 7, amplitude and timescale results are shown for a range of different iceberg dimensions (100 m $\leq H_C \leq$ 1 km, 0.2 $H_C \leq L_C \leq$ 0.7 H_C, $W_C \leq$ 5 km). The model has difficulty matching timescales especially for the larger events (see Figure 7) since maximum amplitude scales approximately as $A \propto T^6$ as expected from equations (15) and (16) with $L \propto H$ (maintaining approximately constant aspect ratio). Unlike the too short timescale problem for class I models, however, the too long timescale problem cannot be solved by calling upon a rate-limiting process working in parallel; but the timescale may be reduced if, for

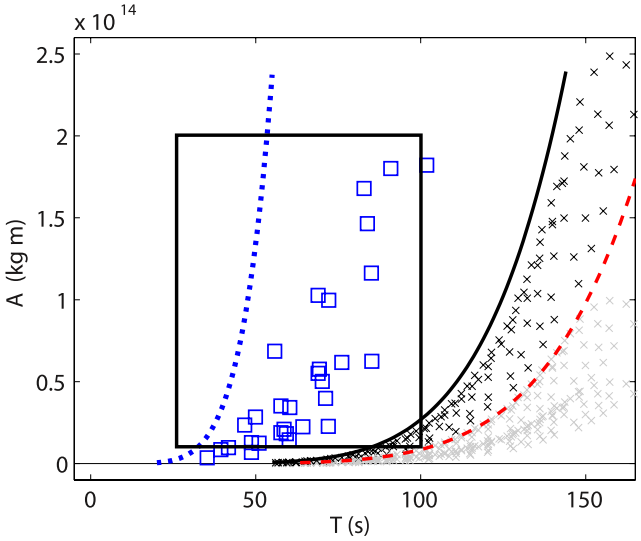

Figure 7. Timescale versus amplitude for model class II (iceberg calving). Black crosses represent different model runs with W_C = 5 km and different values of H_C and L_C (see text) for model IIA (no mélange). Gray crosses are versions of the same runs with W_C scaled down. The blue squares represent different model runs with W_C = 2 km and different values of H_C, L_C, and M_M for model IIB (with mélange). The dashed red line is the scaling of equations (15) and (16) for model IIA with $L_C = H_C/2$ and W_C = 5 km. The solid black line is the same scaling as the dashed red line, but scaled up to approximately denote the cutoff below which timescale/amplitude pairs are possible for model IIA. The dotted blue line is the scaling of equations (15) and (27) for model IIB with $L_C = H_C/2$ and W_C = 2 km. The rectangular box denotes an estimate of the range of observed glacial earthquakes. Model IIB clearly fits observations better than model IIA.

Table 2. Linear Response of Amplitude and Timescale to Tipping Iceberg Parameters

Parameter	Amplitude Response (kg m/km)	Timescale Response (s/km)
H_C	18×10^{13}	34
W_C	0.6×10^{13}	0
L_C	3.8×10^{13}	−174

example, the iceberg loses contact with the glacier face earlier than expected from this simple calculation. As in class I models, the dependence of amplitude and timescale on the parameters is nonlinear but we can linearize and obtain the first-order response away from the above chosen values. This linear response is given in Table 2.

3.2.2. Model IIB: Inclusion of Effective Mass From Ice Mélange

[49] As discussed in section 2.4, there are potentially a number of variations on this calving model. Using, for example, the modification of equation (17) instead of equation (13), we find a parameter regime in which the timescale of the large amplitude calving-contact force is not set by the rotational timescale of equation (16) but is instead set by the timescale of iceberg bobbing given approximately by

$$T \approx 2\pi\sqrt{\frac{H_C}{g}}. \tag{27}$$

[50] In particular, when initial conditions are significantly different from neutrally buoyant, the calving-contact force still develops on the tipping timescale of equation (16). However, the force is strongly modulated by the bobbing timescale of equation (27), sometimes resulting in a force with dominant period set by the bobbing timescale. With this much shorter timescale, a reasonable fit to observations can be produced with the less extreme parameter choice $H_C = 700$ m, $W_C = 2$ km, $L_C = 210$ m, and $M_M = 1.5\ M_C$. As shown in Figure 7 (squares), even with a smaller range of parameter choices than used in model IIA (200 m $\leq H_C \leq$ 1 km, $0.2\ H_C \leq L_C \leq 0.5\ H_C$, $W_C \leq 2$ km, $0.5\ M_C \leq M_M \leq 4\ M_C$), amplitudes and timescales fit better in the observational range.

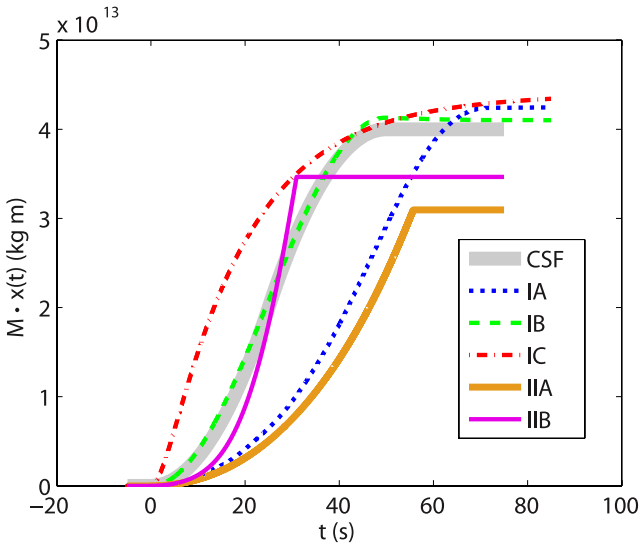

Figure 8. Cumulative centroid single force (CSF) amplitude for: the seismic model fitting the observations (CSF), the three variations on the model class I (IA, IB, and IC), and model class II (IIA and IIB). All five model results are consistent with the CSF model used to model seismic observations (see Figure 10).

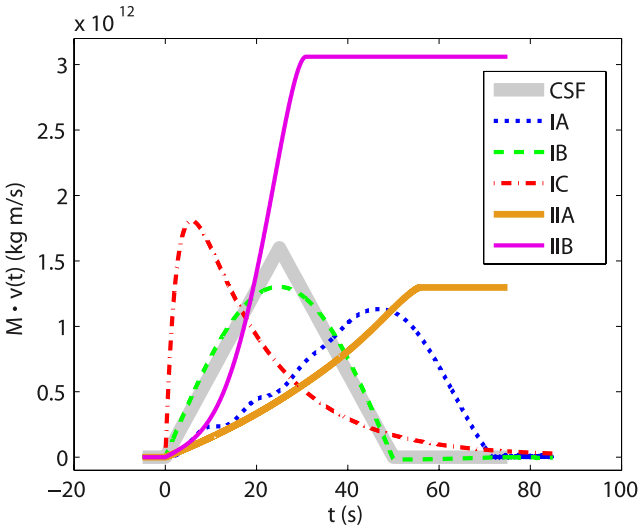

Figure 9. CSF rate for: the seismic model fitting the observations (CSF), the three variations on the model class I (IA, IB, and IC), and model class II (IIA and IIB). Model class II does not have a deceleration phase, so the CSF rate does not return to zero. However, the horizontal portion of the curve does not contribute to the CSF amplitude.

3.3. Model Comparison

[51] The seismic forces predicted by Models IA, IB, IC, IIA and IIB, with parameter choices as described above, are shown in Figure 8 [cumulative CSF amplitude, $A(t)$) and Figure 9 [CSF rate, $\dot{A}(t)$]. Since the current seismic data can be equally well modeled with asymmetric forces of the same characteristic CSF amplitude and timescale (see Figure 10), this data cannot distinguish between the four model possibilities. In addition to satisfying observational constraints 2–4 (see section 1), all models also correctly predict observations 6 and 7. Observation 6 is satisfied since the calving fronts of the glaciers in question have moved substantially over the past 15 years [*Joughin et al.*, 2004; *Howat et al.*, 2005; *Luckman et al.*, 2006] and all models are expected to generate their seismic signal near the calving front. Observation 7 is satisfied since the different glaciers have different model parameter values and therefore the models predict different characteristic amplitudes. The exact values, however, are not constrained well enough for us to decide whether the magnitude (or even the sign) of the variations are correctly modeled in detail. It is somewhat more complicated to compare the models with the final observational constraint 5 since 5 (likely) involves a number of factors that are not completely understood. However, the fact that calving is well known to vary seasonally, while outlet glacier flow is more steady [*Echelmeyer and Harrison*, 1990; *Joughin et al.*, 2008b], and with respect to local glacier conditions strongly suggests that model class II can be expected to produce events in accord with constraint 5 but perhaps not in a predictable sense. Furthermore, adding a simple time-

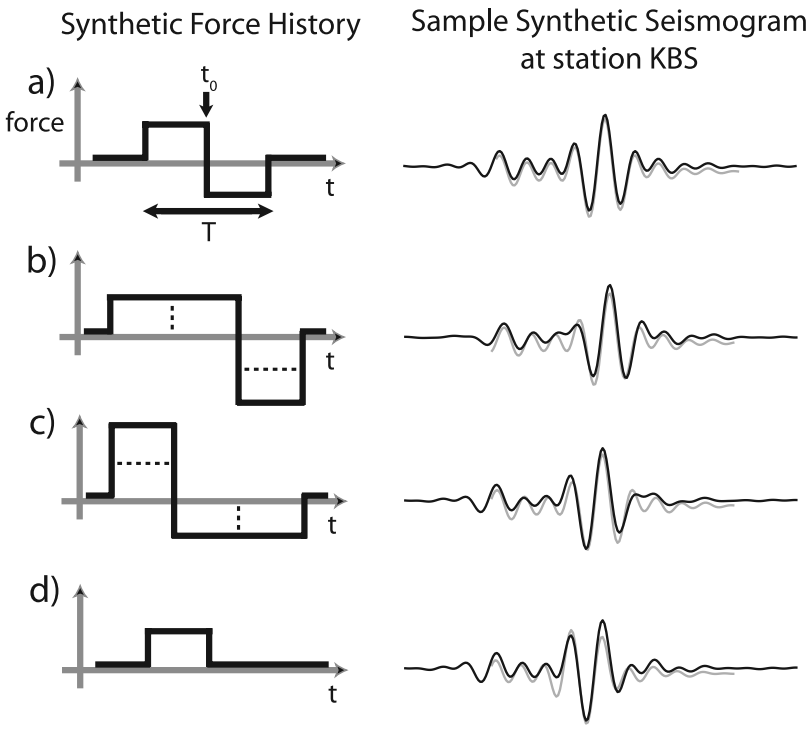

Figure 10. Synthetic force histories and associated synthetic seismograms for (a) the symmetric CSF used to fit the seismic observations, (b) an asymmetric CSF with a longer but lower-amplitude acceleration and shorter high-amplitude deceleration, (c) an asymmetric CSF model with opposite character to the one shown in Figure 10b, and (d) forcing with only an acceleration phase. Synthetic seismograms (black lines) are modeled and filtered as in the paper by *Tsai and Ekström* [2007]; gray lines are the best fit CSF to the synthetic data, offset slightly vertically for clarity. The case shown in Figure 10a corresponds roughly with model IB, the case shown in Figure 10b corresponds roughly with model IA, the case shown in Figure 10c corresponds roughly with model IC, and the case shown in Figure 10d corresponds roughly with model II. All four models fit observations with residual variance (normalized misfit) less than 0.10, compared with typical residual variance on real data of between 0.3 and 0.5. The amplitudes of Figures 10b and 10c are approximately twice that of Figure 10a, and the amplitude of Figure 10d is approximately half that of Figure 10a.

dependent crevassing criterion (i.e., larger, more numerous crevasses during warm periods) to the class I models can produce variations in event size and number that also agrees with the observation that more events but slightly smaller ones occur during warmer times [*Tsai and Ekström*, 2007]. However, the details of such a criterion likely involve the understanding of the calving (and precalving) process in more depth than is currently known. Thus, we do not attempt to model this time dependence in any (more) realistic manner. Model class I may also be able to satisfy constraint 5 if basal processes vary seasonally, as some studies might suggest [e.g., *Kamb et al.*, 1985; *Zwally et al.*, 2002] (although other studies suggest minimal seasonal variations of these processes [*Echelmeyer and Harrison*, 1990; *Truffer et al.*, 2006; *Joughin et al.*, 2008b]).

[52] In summary, we have assembled a unified model of short-timescale outlet glacier dynamics that includes both changes in flow and calving in a physical way. Taking parameter values in the range of reasonable, with the important caveat that a number of important parameters have very loose constraints, we find only five classes (here called IA, IB, IC, IIA and IIB) of models (or a combination) that are able to satisfy the primary observations 1–4. After adding a simple parameterization of time-dependent crevassing (or of basal processes), we find that all five classes of models are able to successfully model all current observations 1–8. It is therefore difficult to decide which of the five possibilities is closer to reality. However, if viscoelastic parameters are thought to be within 1 order of magnitude of the nominal values, then models IA, IIA or IIB should be favored over models IB and IC. Although model IIA has trouble producing the entire range of observations, it does not have as many free parameters as model IA. Furthermore, a slight modification of model IIA resulting in model IIB has only one additional free parameter (the mass of the iceberg mélange) but agrees well with the primary observations. For this reason, we favor model class II.

4. Predictions of the Models and Future Observational Constraints

[53] So far, we have focused on constructing five classes of models that are consistent with observations but it is perhaps the consequences and predictions of the models that are more interesting and can (someday) potentially definitively distinguish the correct mechanism from the incorrect

ones. The first obvious difference among models is that model class I requires motion of the glacier itself whereas model class II requires motion of a calved iceberg and glacier motion is secondary. Thus, observations of glacier and/or iceberg motion (of the magnitudes discussed in section 3) coincident with a glacial earthquake event (or lack of such motion) would be diagnostic of either model class I or II. Recent GPS observations from the Helheim and Jakobshavn glaciers [*Nettles et al.*, 2007; *Fahnestock et al.*, 2007] suggest that little surface motion occurs during glacial earthquakes, thereby arguing against model class I. The other obvious difference between all five models is the exact form of the force history on the Earth (see Figure 8). However, these differences are not large enough to be distinguished from modeling of global seismic data and would therefore require modeling of high-quality, local seismic data.

[54] Another set of differences that is more promising in terms of distinguishing between models is the difference in bulk viscoelastic parameters required by the different models. As discussed in section 3.3, models IA and II do not require great differences from the nominal values whereas models IB and IC do (model IB with μ_2 1000 times smaller than nominal; model IC with μ_1 80 times smaller and η_1 2000 times smaller). In situ bulk viscoelastic parameters are difficult to measure but could possibly be done with a combination of tidal flexure [*Vaughan*, 1995] on outlet glaciers with a significant floating tongue, high-precision GPS on highly variable-velocity outlet glaciers [e.g., *Bindschadler et al.*, 2003], and in situ measurements of temperature and the degree of internal small-scale fracturing. Fracturing and crevassing in general is predicted to be different among the models. As discussed in section 2.2, s trades off directly with viscoelastic parameters so that bulk differences in (lower values of) viscoelastic parameters may be a result of differences in (lower values of) s. Thus, models requiring very low bulk viscoelastic parameters may be expected to have large amounts of crevassing and fracture. Additionally, it is possible that crevassing affects different viscoelastic parameters differently, so that crevassing could possibly be responsible for all differences in viscoelastic parameters. Furthermore, if time-dependent crevassing is partially responsible for allowing (large) glacial earthquakes to occur then one might expect to observe many micro-earthquakes associated with the cracking [e.g., *Neave and Savage*, 1970; *O'Neel et al.*, 2007], either seasonally or concurrently with the earthquake events. However, extensive crevassing of the sort considered would probably be meltwater driven, and may not have a seismic signature if the process is too slow.

[55] If model class II is correct, one would also expect related short-period seismicity related to cracking events that accompany calving as has been observed in analogous outlet glaciers in Alaska [*Qamar*, 1988; *O'Neel et al.*, 2007]. Furthermore, visual observations (like those of *Truffer et al.* [2006] and J. Amundson (private communication, 2008)) of calving coincident with glacial earthquakes would be diagnostic of model class II. Model IIB would additionally predict glacial earthquakes only occurring when the glacier fjord has substantial iceberg mass, another potential visual or satellite observable. Model IIB could thus explain the lack of glacial earthquakes at Columbia Glacier, where large icebergs calve but there is little ice mélange.

[56] Finally, one should remember that the most incomplete part of model class I is the part regarding the basal processes leading to $f(t)$. The reason for this incompleteness is the vastly inadequate knowledge of the factors most important to determining $f(t)$. There are currently only suggestions [*Iken*, 1981; *Kamb*, 1991; *Schoof*, 2005] that the variations in $f(t)$ needed for these models to work can be produced by physical processes. Thus, basal observations would greatly improve our ability to form a predictive model class I. For example, determining whether till deformation or basal sliding contributes more to steady state velocities would narrow the myriad of possibilities for basal instabilities substantially, therefore making the modeling of $f(t)$ more tractable. Having a more physical model of $f(t)$ could in turn yield additional predictions for class I model behavior. While possibly irrelevant to the types of glacial earthquakes discussed here, the basal mechanisms of class I models are presumably important to other types of episodic glacial motion.

5. Conclusions

[57] Using available observational constraints, we have constructed a general model framework to understand very short timescale (<100 s) variability at the calving margin of fast-flowing outlet glaciers. Since key variables are unknown, we find it necessary to parameterize several processes within the model framework. Under this framework, we are able to construct five classes of models that result in instabilities that match known observations of glacial earthquakes. Although current observations cannot definitively rule out any of possibilities, model class II (iceberg calving) has fewer adjustable parameters, requires more realistic parameter choices, and is significantly more consistent with observations. The addition of iceberg mélange (model IIB) further improves the consistency of model class II with observations (at the cost of an added free parameter). We therefore strongly favor model class II but reserve final judgment for the future, when observations should be able to conclusively distinguish among the model classes.

Appendix A

A1. Approximate Timescale for Calved Iceberg to Slide Down to Equilibrium

[58] To arrive at the timescale of a calved iceberg sliding freely on a bed with positive slope β, we note that under hydrostatic water pressure (including along the bed) the net force in the downslope direction is

$$F = \rho g H_C W_C L_C \sin\beta - \rho_w g W_C L_C \tan\beta \cdot \Delta h \qquad \text{(A1)}$$

where Δh is the height to the water surface level as measured from the middle of the base of the iceberg (see Figure 5b), and the iceberg is assumed to be a rectangular block of height H_C, length L_C, and width W_C parallel to the bed. Defining x along the bed to be positive in the downstream direction and $x = 0$ where $\Delta h = 0$ then $\Delta h = x \sin\beta$ so that

$$F(x) = g W_C L_C \sin\beta \cdot (\rho H_C - \rho_w \tan\beta \cdot x). \qquad \text{(A2)}$$

[59] Defining x_0 to be the point at which the driving force vanishes, then $\rho H_C = \rho_w \tan\beta \cdot x_0$ and

$$F(x) = \rho_w g W_C L_C \sin\beta \tan\beta \cdot (x_0 - x). \tag{A3}$$

[60] Substituting (A3) into Newton's second law gives

$$\rho_w g W_C L_C \sin\beta \tan\beta \cdot (x_0 - x) = \rho W_C L_C H_C \cdot \ddot{x} \tag{A4}$$

which, with initial conditions x_0-$x(0) = x_1$ and $\dot{x}(0) = 0$, has solution

$$x(t) = x_0 - x_1 \cos(\pi \cdot t/T) \tag{A5}$$

with timescale given by

$$T = \pi\sqrt{\frac{\rho H_C \cos\beta}{\rho_w g \sin^2\beta}}. \tag{A6}$$

[61] The above analysis is only true as long as the top-forward corner of the iceberg is not submerged, or equivalently

$$x \sin\beta < H_C \cos\beta - \frac{L_C}{2}\sin\beta. \tag{A7}$$

[62] Taking $x_1 \ll x_0$ then the solution (A5) is valid as long as $x = x_0$ satisfies (A7) or

$$\tan\beta < \left(1 - \frac{\rho}{\rho_w}\right)\frac{2H_C}{L_C} \approx \frac{H_C}{5L_C} \tag{A8}$$

which is true since $\beta \ll 1$. This analysis yields a lower-bound estimate of the timescale since it assumes water freely moves to maintain hydrostatic balance.

A2. Rotational Iceberg Calving Model

[63] As in the paper by *MacAyeal et al.* [2003], we assume the forces on the iceberg are (1) hydrostatic water pressure $p_w = \rho_w g \times$ depth applied at all submerged surfaces, (2) gravitational weight of the iceberg $gM_C = \rho g H_C W_C L_C$, and (3) calving-contact force from the glacier face F_C (and from the iceberg mélange F_{C2} in model IIB) (see Figure 6). Instead of solving for equilibrium conditions, these forces are then inputted into equations (10), (11), and (12). Forces from water pressure in the x direction cancel out, leaving F_x as a sum of contact forces. (With no iceberg mélange $F_C = -F_x$.) Accounting for weight and vertical pressure forces, where y_i is the water depth of the center of mass of the iceberg, F_y is given by either

$$F_y = gM_C\left(1 - \frac{\rho_w}{2\rho} - \frac{\rho_w y_i}{\rho H_C \cos\theta}\right) \tag{A9}$$

when the top two corners of the iceberg are unsubmerged or

$$F_y = gM_C\left(1 - \frac{\rho_w}{\rho} + \frac{\rho_w(H_C\cos\theta + L_C\sin\theta - 2y_i)^2}{8\rho H_C L_C \sin\theta\cos\theta}\right) \tag{A10}$$

when only one corner is unsubmerged. Similarly, τ_{rot} is given by

$$\tau_{rot} = -(F_C r_\perp + F_{C2} r_\perp) + \int_{submerged} p_w r_\perp dA = -\tau_{rot1} + \tau_{rot2} \tag{A11}$$

where $r_\perp$ is closest distance to the center of mass of the line of action of the force,

$$\tau_{rot1} = \frac{H_C}{2}F_C\frac{2M_{xa} - M_{xa0}}{M_{xa}}\left(\cos\theta - \frac{L_C}{H_C}\sin\theta\right), \tag{A12}$$

and τ_{rot2} is given by either

$$\tau_{rot2} = M_C g H_C \frac{\rho_w \sin\theta}{\rho\cos^2\theta}\left[\frac{1}{8}\cos^2\theta - \frac{y_i^2}{2H_C^2} - \frac{L_C^2}{24H_C^2}\left(1 + \cos^2\theta\right)\right] \tag{A13}$$

when the top two corners of the iceberg are unsubmerged or

$$\tau_{rot2} = \frac{\rho_w g W_C}{6}\left(y_i - \frac{H_C}{2}\cos\theta - \frac{L_C}{2}\sin\theta\right)^2 \left[\frac{\sin^2\theta - \cos^2\theta}{\cos^2\theta\sin^2\theta}y_i + \frac{H_C}{\cos\theta} - \frac{L_C}{\sin\theta} + \frac{H_C\cos\theta}{2\sin^2\theta} - \frac{L_C\sin\theta}{2\cos^2\theta}\right] \tag{A14}$$

when only one corner is unsubmerged. Note that τ_{rot1} accounts for the torque from the contact forces, τ_{rot2} accounts for the torque from the water pressure. Finally, to close the system of equations, we have the contact constraint

$$x_i = \frac{1}{2}(H_C \sin\theta + L_C \cos\theta). \tag{A15}$$

[64] Combining equations (10), (12), (A11), and (A15) results in an equation of the form

$$A(\theta)\ddot{\theta} = B(\theta)\dot{\theta}^2 + C(\theta, y_i) \tag{A16}$$

which, along with equations (11), (A9), and (A10), are a 2-D system of equations in the variables θ and y_i that are then solved numerically. Initial conditions are chosen with small but nonzero θ ($0.1 \le \theta \le 0.15$ radians) to ensure eventual tipping of the iceberg, and a range of initial y_i including that for a neutrally buoyant iceberg. Since the seismic response is only sensitive to large values of CSF rate, $\dot{A}$, the A and T reported are for the time range when $\dot{A}$ is a significant fraction of the maximum value of $\dot{A}$ attained (e.g., $\dot{A} \ge 0.2\ \max[\dot{A}]$).

A3. Analytic Approximation for Purely Elastic Response

[65] To arrive at an analytic approximation for the purely elastic response, we perform a force balance on the glacier block of mass $M = \rho HWL$ that is initially held by friction f_0, which drops to zero along the base over a length ΔL, and is then allowed to move as constrained by elastic elements at its side margins and upstream end. As in section 2.6, balancing gravitational driving force against basal friction plus the force

accommodated by Glen's law at the margins (over length scale W_S) yields an expression for the steady state basal friction

$$f_0 = \alpha - \frac{2s}{\rho g W}\left(\frac{u_{ss}}{2W_S A_{Gl}}\right)^{1/3}. \quad \text{(A17)}$$

[66] Allowing this friction to drop to zero over length ΔL gives a force perturbation

$$\Delta F = f_0 \Delta M g = f_0 \rho g H W \Delta L. \quad \text{(A18)}$$

[67] The elastic force from displacing Δx with marginal shear (over two sides of width W_S) and longitudinal stretching (over one side of length L_S, with elastic modulus approximately three times that of the shear modulus) is

$$F_E(\Delta x) = E\Delta x = sWH\left(3\mu_2\frac{\Delta x}{L_S}\right) + 2sLH\left(\mu_2\frac{\Delta x}{W_S}\right). \quad \text{(A19)}$$

[68] The glacier block then satisfies the simple differential equation

$$M\Delta\ddot{x} + E\Delta x = \Delta F \quad \text{(A20)}$$

which has a simple sinusoidal solution with amplitude and timescale given by

$$\Delta x_{\max} = 2\Delta F/E \quad \text{(A21)}$$

and

$$T = \text{Period}/2 = \pi\sqrt{\frac{M}{E}} \quad \text{(A22)}$$

so that the CSF amplitude $A = M\Delta x_{\max}$ and timescale are given by

$$A = \frac{\rho^2 g H W^2 W_S \cdot \Delta L}{s\mu_2[1 + 3WW_S/(2LL_S)]} \cdot \left[\alpha - \frac{2s}{\rho g W}\left(\frac{u_{ss}}{2W_S A_{Gl}}\right)^{1/3}\right] \quad \text{(A23)}$$

and

$$T = \pi\sqrt{\frac{2\rho WW_S LL_S}{s\mu_2(3WW_S + 2LL_S)}}. \quad \text{(A24)}$$

Notation

a	glacier half width.
A	CSF amplitude of glacial earthquake.
A_{Gl}	Glen's rate parameter.
e_{ij}	deviatoric strain tensor.
E	effective elastic constant.
f	dimensionless basal shear strength.
F_0	initial dimensionless shear strength.
F_B	basal force.
F_C	calving force.
F_D	driving force.
F_E	general elastic force.
F_L	longitudinal ice deformation force.
F_M	marginal ice deformation force.
F_x	force in x direction on calved iceberg.
F_y	force in y direction on calved iceberg.
g	gravitational acceleration.
H	height of glacier block.
H_C	height of calved iceberg.
H_{crev}	effective height of crevassing.
H_S	height of basal shear zone.
L	length of glacier block.
L_C	length of calved iceberg.
L_S	length of longitudinal deformation zone.
M	mass of glacier block.
M_C	mass of iceberg.
M_M	mass of entrained iceberg mélange.
M_S	conventional surface wave magnitude.
M_{SW}	surface wave magnitude measured at 35–150 s.
M_{xa}	effective mass of iceberg moving in x direction.
M_{ya}	effective mass of iceberg moving in y direction.
n	Glen's law exponent.
p_{eff}	effective pressure.
p_{ice}	ice pressure.
p_w	water pressure.
s	fraction of height with rheology applied.
t	time.
T	CSF timescale of glacial earthquake.
$u(r)$	transverse velocity profile.
u_{ss}	steady state background block velocity.
W	width of glacier block.
W_C	width of iceberg.
W_S	width of marginal shear deformation zone.
x	distance in the along-glacier direction.
x_1	displacement initial condition in Appendix 1.
x_b	displacement of glacier block.
x_{b0}	displacement initial condition of glacier block.
x_i	horizontal displacement of iceberg.
x_{i0}	horizontal displacement initial condition.
y_i	vertical displacement of iceberg.
y_{i0}	vertical displacement initial condition.
α	glacier surface slope.
β	glacier bed slope.
Δh	height of water.
ΔL	length of basal instability.
Δx	general elastic displacement.
$\Delta x_{\max}$	maximum of general elastic displacement.
ε_{ij}	strain tensor.
η_1	viscosity of Kelvin element.
η_2	viscosity of Maxwell element.
μ_1	shear modulus of Kelvin element.
μ_2	shear modulus of Maxwell element.
μ_{2eff}	effective shear modulus of Maxwell element.
ν	Poisson's ratio.
ρ	ice density.
ρ_w	water density.
σ	standard deviation.
σ_{ij}	stress tensor.
τ	Huber-Mises equivalent shear stress.
τ_{ij}	deviatoric stress tensor.
τ_{rot}	torque on iceberg through center of mass.
θ	angle of rotation of iceberg.
$\dot{x}$	time derivative of quantity x.
$\ddot{x}$	second time derivative of quantity x.

[69] **Acknowledgments.** We thank I. Joughin, R. B. Alley, I. M. Howat, M. Nettles, and G. Ekström for helpful discussion, and we thank S. O'Neel, M. Truffer, and S. Tulaczyk for constructive reviews. This work was supported by a National Science Foundation Graduate Research Fellowship to V.C.T. and, in its later stages, by NSF-OPP grant ANT-0739444.

References

Anandakrishnan, S., and R. B. Alley (1997), Tidal forcing of basal seismicity of ice stream C, West Antarctica, observed far inland, *J. Geophys. Res.*, *102*, 15,183–15,196, doi:10.1029/97JB01073.

Anandakrishnan, S., and C. R. Bentley (1993), Micro-earthquakes beneath ice stream-B and ice stream-C, West Antarctica - Observations and implications, *J. Glaciol.*, *39*, 455–462.

Bamber, J. L., R. L. Layberry, and S. P. Gogineni (2001), A new ice thickness and bed data set for the Greenland ice sheet 1. Measurement, data reduction, and errors, *J. Geophys. Res.*, *106*, 33,773–33,780, doi:10.1029/2001JD900054.

Bindschadler, R. A., M. A. King, R. B. Alley, S. Anandakrishnan, and L. Padman (2003), Tidally controlled stick-slip discharge of a West Antarctic ice stream, *Science*, *301*, 1087–1089, doi:10.1126/science.1087231.

Brennen, C. E. (1982), A review of added mass and fluid inertial forces, *Tech. Rep. CR82.010*, Nav. Civ. Eng. Lab., Dep. of the Navy, Port Hueneme, Calif.

Budd, W. F., and T. H. Jacka (1989), A review of ice rheology for ice sheet modeling, *Cold Reg. Sci. Technol.*, *16*, 107–144, doi:10.1016/0165-232X(89)90014-1.

Dahlen, F. A. (1993), Single-force representation of shallow landslide sources, *Bull. Seismol. Soc. Am.*, *83*, 130–143.

Das, S. B., I. Joughin, M. D. Behn, I. M. Howat, M. A. King, D. Lizarralde, and M. P. Bhatia (2008), Fracture propagation to the base of the Greenland ice sheet during supraglacial lake drainage, *Science*, *320*, 778–781, doi:10.1126/science.1153360.

Deichmann, N., J. Ansorge, F. Scherbaum, A. Aschwanden, F. Bernardi, and G. H. Gudmundsson (2000), Evidence for deep icequakes in an Alpine glacier, *Ann. Glaciol.*, *31*, 85–90, doi:10.3189/172756400781820462.

Dieterich, J. H. (1994), A constitutive law for rate of earthquake production and its application to earthquake clustering, *J. Geophys. Res.*, *99*, 2601–2618, doi:10.1029/93JB02581.

Echelmeyer, K. A., and W. D. Harrison (1990), Jakobshavn Isbrae, West Greenland: Seasonal variations in velocity - Or lack thereof, *J. Glaciol.*, *36*, 82–88.

Ekström, G. (2006), Global detection and location of seismic sources by using surface waves, *Bull. Seismol. Soc. Am.*, *96*, 1201–1212, doi:10.1785/0120050175.

Ekström, G., M. Nettles, and G. A. Abers (2003), Glacial earthquakes, *Science*, *302*, 622–624, doi:10.1126/science.1088057.

Ekström, G., M. Nettles, and V. C. Tsai (2006), Seasonality and increasing frequency of Greenland glacial earthquakes, *Science*, *311*, 1756–1758, doi:10.1126/science.1122112.

Fahnestock, M., M. Truffer, M. Luthi, R. Motyka, J. Amundson, and J. Brown (2007), GPS and conventional surveying measurement of glacier and iceberg motion in the Jakobshavns Isbrae system, *Eos Trans. AGU*, *88*(52), Fall Meet. Suppl., Abstract G33C-03.

Fountain, A. G., R. W. Jacobel, R. Schlichting, and P. Jansson (2005), Fractures as the main pathways of water flow in temperate glaciers, *Nature*, *433*, 618–621, doi:10.1038/nature03296.

Glen, J. W. (1955), The creep of polycrystalline ice, *Proc. R. Soc. London, Ser. A*, *228*, 519–538, doi:10.1098/rspa.1955.0066.

Harper, J. T., N. F. Humphrey, W. T. Pfeffer, T. Fudge, and S. O'Neel (2005), Evolution of subglacial water pressure along a glacier's length, *Ann. Glaciol.*, *40*, 31–36, doi:10.3189/172756405781813573.

Harrison, W. D., K. A. Echelmeyer, and C. F. Larson (1998), Measurement of temperature in a margin of ice stream, Antarctica: Implications for margin migration and lateral drag, *J. Glaciol.*, *44*, 615–624.

Howat, I. M., I. Joughin, S. Tulaczyk, and S. Gogineni (2005), Rapid retreat and acceleration of Helheim glacier, east Greenland, *Geophys. Res. Lett.*, *32*, L22502, doi:10.1029/2005GL024737.

Iken, A. (1981), The effect of the subglacial water pressure on the sliding velocity of a glacier in an idealized numerical model, *J. Glaciol.*, *27*, 407–421.

Iken, A., H. Rothlisberger, A. Flotron, and W. Haeberli (1983), The uplift of Unteraargletscher at the beginning of the melt season - A consequence of water storage at the bed?, *J. Glaciol.*, *29*, 28–47.

Iken, A., K. Echelmeyer, W. Harrison, and M. Funk (1993), Mechanisms of fast flow in Jakobshavns Isbrae, West Greenland: Part I. Measurements of temperature and water level in deep boreholes, *J. Glaciol.*, *39*, 15–25.

Jellinek, H. H. G., and R. Brill (1956), Viscoelastic properties of ice, *J. Appl. Phys.*, *27*, 1198–1209, doi:10.1063/1.1722231.

Joughin, I., W. Abdalati, and M. Fahnestock (2004), Large fluctuations in speed on Greenland's Jakobshavn Isbrae glacier, *Nature*, *432*, 608–610, doi:10.1038/nature03130.

Joughin, I., I. Howat, R. B. Alley, G. Ekström, M. Fahnestock, T. Moon, M. Nettles, M. Truffer, and V. C. Tsai (2008a), Ice-front variation and tidewater behavior on Helheim and Kangerdlugssuaq glaciers, Greenland, *J. Geophys. Res.*, *113*, F01004, doi:10.1029/2007JF000837.

Joughin, I., S. B. Das, M. A. King, B. E. Smith, I. M. Howat, and T. Moon (2008b), Seasonal speedup along the western flank of the Greenland ice sheet, *Science*, *320*, 781–783, doi:10.1126/science.1153288.

Kalifa, P., G. Ouillon, and P. Duval (1992), Microcracking and the failure of polycrystalline ice under triaxial compression, *J. Glaciol.*, *38*, 65–76.

Kamb, B. (1991), Rheological nonlinearity and flow instability in the deforming bed mechanism of ice stream motion, *J. Geophys. Res.*, *96*, 16,585–16,595, doi:10.1029/91JB00946.

Kamb, B., and H. Engelhardt (1987), Waves of accelerated motion in a glacier approaching surge: The mini-surges of Variegated Glacier, Alaska, USA, *J. Glaciol.*, *33*, 27–46.

Kamb, B., C. F. Raymond, W. D. Harrison, H. Engelhardt, K. A. Echelmeyer, N. Humphrey, M. M. Brugman, and T. Pfeffer (1985), Glacier surge mechanism: 1982–1983 surge of Variegated Glacier, Alaska, *Science*, *227*, 469–479, doi:10.1126/science.227.4686.469.

Kamb, B., H. Engelhardt, M. A. Fahnestock, N. Humphrey, M. Meier, and D. Stone (1994), Mechanical and hydrologic basis for the rapid motion of a large tidewater glacier: 2. Interpretation, *J. Geophys. Res.*, *99*, 15,231–15,244, doi:10.1029/94JB00467.

Kawakatsu, H. (1989), Centroid single force inversion of seismic waves generated by landslides, *J. Geophys. Res.*, *94*, 12,363–12,374, doi:10.1029/JB094iB09p12363.

Lamb, H. (1953), *Hydrodynamics*, 6th ed., Cambridge Univ. Press, New York.

Lapusta, N., J. R. Rice, Y. Ben-Zion, and G. Zheng (2000), Elastodynamic analysis for slow tectonic loading with spontaneous rupture episodes on faults with rate- and state-dependent friction, *J. Geophys. Res.*, *105*, 23,765–23,789, doi:10.1029/2000JB900250.

Liu, Y., and J. R. Rice (2007), Spontaneous and triggered aseismic transient deformation in a subduction fault model, *J. Geophys. Res.*, *112*, B09404, doi:10.1029/2007JB004930.

Luckman, A., T. Murray, R. de Lange, and E. Hanna (2006), Rapid and synchronous ice-dynamic changes in east Greenland, *Geophys. Res. Lett.*, *33*, L03503, doi:10.1029/2005GL025428.

MacAyeal, D. R., T. A. Scambos, C. L. Hulbe, and M. A. Fahnestock (2003), Catastrophic ice-shelf break-up by an ice-shelf-fragment-capsize mechanism, *J. Glaciol.*, *49*, 22–36, doi:10.3189/172756503781830863.

MacAyeal, D. R., M. H. Okal, J. E. Thom, K. M. Brunt, Y. J. Kim, and A. K. Bliss (2008), Tabular iceberg collisions within the coastal regime, *J. Glaciol.*, *54*, 371–386, doi:10.3189/002214308784886180.

Milne-Thomson, L. M. (1955), *Theoretical Hydrodynamics*, 3rd ed., Macmillan, New York.

Neave, K. G., and J. C. Savage (1970), Icequakes on Athabasca Glacier, *J. Geophys. Res.*, *75*, 1351–1362, doi:10.1029/JB075i008p01351.

Nettles, M., et al. (2007), Short-time-scale variations in flow speed and behavior, Helheim Glacier, East Greenland, *Eos Trans. AGU*, *88*(52), Fall Meet. Suppl., Abstract C13A-08.

Nye, J. F. (1965), The flow of a glacier in a channel of rectangular, elliptic or parabolic cross-section, *J. Glaciol.*, *5*, 661–690.

O'Neel, S., H. P. Marshall, D. E. McNamara, and W. T. Pfeffer (2007), Seismic detection and analysis of icequakes at Columbia Glacier, Alaska, *J. Geophys. Res.*, *112*, F03S23, doi:10.1029/2006JF000595.

Paterson, W. S. B. (2002), *The Physics of Glaciers*, 3rd ed., Elsevier, Oxford, U.K.

Qamar, A. (1988), Calving icebergs: A source of low-frequency seismic signals from Columbia Glacier, Alaska, *J. Geophys. Res.*, *93*, 6615–6623, doi:10.1029/JB093iB06p06615.

Rist, M. A., P. R. Sammonds, S. A. F. Murrell, P. G. Meredith, C. S. M. Doake, H. Oerter, and K. Matsuki (1999), Experimental and theoretical fracture mechanics applied to Antarctic ice fracture and surface crevassing, *J. Geophys. Res.*, *104*, 2973–2987, doi:10.1029/1998JB900026.

Ruina, A. (1983), Slip instability and state variable friction laws, *J. Geophys. Res.*, *88*, 10,359–10,370, doi:10.1029/JB088iB12p10359.

Schoof, C. (2005), The effect of cavitation on glacier sliding, *Proc. R. Soc., Ser. A*, *461*, 609–627, doi:10.1098/rspa.2004.1350.

Schulson, E. M. (2001), Brittle failure of ice, *Eng. Fract. Mech.*, *68*, 1839–1887, doi:10.1016/S0013-7944(01)00037-6.

Smith, A. M. (2006), Microearthquakes and subglacial conditions, *Geophys. Res. Lett.*, *33*, L24501, doi:10.1029/2006GL028207.

Stuart, G., T. Murray, A. Brisbourne, P. Styles, and S. Toon (2005), Seismic emissions from a surging glacier: Bakaninbreen, Svalbard, *Ann. Glaciol.*, *42*, 151–157, doi:10.3189/172756405781812538.

Truffer, M., and K. A. Echelmeyer (2003), Of isbrae and ice streams, *Ann. Glaciol.*, *36*, 66–72, doi:10.3189/172756403781816347.

Truffer, M., K. A. Echelmeyer, and W. D. Harrison (2001), Implications of till deformation on glacier dynamics, *J. Glaciol.*, *47*, 123–134, doi:10.3189/172756501781832449.

Truffer, M., J. Amundson, M. Fahnestock, and R. J. Motyka (2006), High time resolution velocity measurements on Jakobshavn Isbrae, *Eos Trans. AGU*, *87*(52), Fall Meet. Suppl., Abstract C11A-1132.

Tsai, V. C., and G. Ekström (2007), Analysis of glacial earthquakes, *J. Geophys. Res.*, *112*, F03S22, doi:10.1029/2006JF000596.

Tsai, V. C., and J. R. Rice (2006), Possible mechanisms for glacial earthquakes, *Eos Trans. AGU*, *87*(52), Fall Meet. Suppl., Abstract C41A-0290.

Tse, S. T., and J. R. Rice (1986), Crustal earthquake instability in relation to the depth variation of frictional slip properties, *J. Geophys. Res.*, *91*, 9452–9472, doi:10.1029/JB091iB09p09452.

Tulaczyk, S., W. B. Kamb, and H. F. Engelhardt (2000), Basal mechanics of ice stream B, West Antarctica 1. Till mechanics, *J. Geophys. Res.*, *105*, 463–481, doi:10.1029/1999JB900329.

van der Veen, C. J. (1998), Fracture mechanics approach to penetration of surface crevasses on glaciers, *Cold Reg. Sci. Technol.*, *27*, 31–47, doi:10.1016/S0165-232X(97)00022-0.

VanWormer, D., and E. Berg (1973), Seismic evidence for glacier motion, *J. Glaciol.*, *12*, 259–265.

Vaughan, D. G. (1995), Tidal flexure at ice shelf margins, *J. Geophys. Res.*, *100*, 6213–6224, doi:10.1029/94JB02467.

Venteris, E. R. (1999), Rapid tidewater glacier retreat: A comparison between Columbia Glacier, Alaska and Patagonian calving glaciers, *Global Planet. Change*, *22*, 131–138, doi:10.1016/S0921-8181(99)00031-4.

Weaver, C. S., and S. D. Malone (1979), Seismic evidence for discrete glacier motion at the rock-ice interface, *J. Glaciol.*, *23*, 171–184.

Wolf, L. W., and J. N. Davies (1986), Glacier-generated earthquakes from Prince William Sound, Alaska, *Bull. Seismol. Soc. Am.*, *76*, 367–379.

Zwally, H. J., W. Abdalati, T. Herring, K. Larson, J. Saba, and K. Steffen (2002), Surface melt-induced acceleration of Greenland ice-sheet flow, *Science*, *297*, 218–222, doi:10.1126/science.1072708.

M. Fahnestock, Institute for the Study of Earth, Oceans, and Space, University of New Hampshire, Durham, NH 03824, USA.

J. R. Rice and V. C. Tsai, Department of Earth and Planetary Sciences, Harvard University, Cambridge, MA 02138, USA. (vtsai@fas.harvard.edu)